Supplementary Material

Davor Curic,[1,*] Donovan Ashby,[2] Alexander McGirr,[2,3,4] and Jörn Davidsen[1,5]

[1] *Complexity Science Group, Department of Physics and Astronomy University of Calgary, Calgary, Alberta T2N 1N4, Canada*
[2] *Department of Psychiatry University of Calgary, Calgary, Alberta T2N 1N4, Canada*
[3] *Hotchkiss Brain Institute, University of Calgary, Calgary, Alberta T2N 4N1, Canada*
[4] *Mathison Centre for Mental Health Research and Education Calgary, Alberta, Canada.*
[5] *Hotchkiss Brain Institute, University of Calgary, Calgary, Alberta T2N 4N1, Canada*

(Dated: August 1, 2024)

S1. Concatenated Statistics

Critical exponents in presented in the main paper are obtained on a per-recording basis. However, for clarity, figures show statistics concatenated to form one curve so that comparison between QW, isoflurane, ketamine, and pentobarbital is visually clear. Fig. S1 shows that the concatenated statistics are fairly representative of individual recordings. Estimation ranges tended to be about an order of magnitude shorter for the concatenated statistics, reflecting the variability across animals. For duration distributions however, which only had typically one order of magnitude of estimation range on a per-recording basis, it was not possible to find a meaningful region where our estimation criterion could be established.

Table SI shows the avalanche size exponents obtained for the concatenated data and agrees fairly well with Table 1 in the main text. These are labeled p-value constrained as the method to get the estimation region requires constraining the p-value to be greater than 0.1. However, its possible that this could lead to differences simply based off where this region is. As such we also test exponent estimates by constraining the fitting domain to the QW estimation domain. This ensures that differences in the exponent do not arise from the choice in domain, but does not guarantee that the p-value of the fitting is significant. Table SI shows that the two methods give similar results

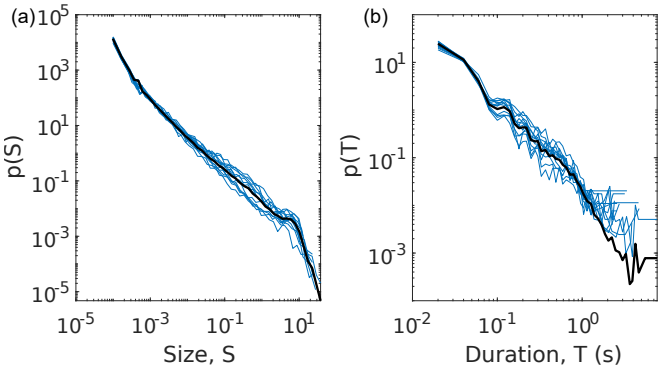

FIG. S1. Per-animal comparison of avalanche statistics. Avalanche size (a) and durations (b) for individual quiet wakefulness recordings ($n = 12$), compared with the concatenated data (black curve). Source data are provided as a Source data file.

condition	p-value constrained	range constrained
QW	1.14(4)	N/A
Iso. 1%	1.16(6)	1.23(4)
Iso. 2%	1.14(4)	1.13(5)
Ket. 10 mg/kg	1.06(4)	1.10(4)
Ket. 100 mg/kg	1.08(5)	1.04(5)
Pent. 12.5 mg/kg	0.93(5)	0.95(3)
Pent. 80 mg/kg	0.89(5)	0.94(4)

TABLE SI. Exponent τ estimated for the different conditions using the p-value and range constrained methods. Brackets denote uncertainty on the last digit.

S2. Avalanche Duration and Scaling Relation

Unlike avalanche sizes, avalanche durations are strictly discrete (i.e., in terms of frames), and their overall range is much shorter (see Fig. S2a) such that a continuous estimator is not a good approximation. In this case a different estimator must be used for maximum likelihood [1]. In particular we use:

$$p(\alpha|T) = \frac{T^{-\alpha}}{\zeta(\alpha, T_{min}) - \zeta(\alpha, 1 + T_{max})}, \qquad \text{(S1)}$$

where $\zeta(\alpha, T_{min})$ is the Hurwitz zeta function. This is the same as the estimator shown in [1], with the added feature that the distribution has a finite upper cutoff T_{max}. The choice of T_{min} and T_{max} is the same as for the avalanche sizes — it is the largest range for which the p-value of a KS-test against a theoretical distribution is above 0.1. Typically these ranges were on the order of a single decade, though this is largely due to the fact that avalanche durations scarcely span over two decades.

We also analyzed the typical avalanche duration for a given avalanche size, written $\langle T \rangle(S)$ (Fig. S2b). This is calculated by finding the mean duration of avalanches in size bins $[S_i, S_{i+1})$. The exponent γ describes the rela-

* dcuric@ucalgary.ca

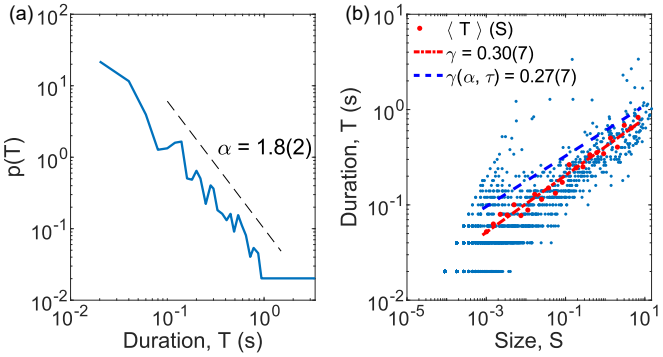

FIG. S2. Avalanche duration analysis. a) Example of avalanche duration distribution in quiet wakefulness for a single recording. The dashed line extends over the estimation region and has a slope α. b) For the same recording, the avalanche duration against avalanche size. Red dots represent the average duration for a given size, $\langle T \rangle(S)$. The estimation for γ via robust linear fitting is shown, as well as the value obtained from the scaling relation, $\gamma(\alpha, \tau)$, given by Eq. 2. Source data are provided as a Source data file.

tionship between S and $\langle T \rangle$ and is calculated by using a robust linear fit (*robustfit*, MATLAB) to the logarithm of both S and $\langle T \rangle$. This value is compared against the $\gamma(\alpha, \tau)$ which is calculated from the scaling relationship in Eq. 2, and the uncertainty $\delta\gamma(\alpha, \tau)$ is calculated from the uncertainties $\delta\tau$ and $\delta\alpha$ via standard error-propagation:

$$\delta\gamma(\alpha,\tau) = \sqrt{\frac{(\alpha-1)^2}{(\tau-1)^4}\delta\tau^2 + \frac{1}{(\tau-1)^2}\delta\alpha^2} \qquad \text{(S2)}$$

S3. Altered Dynamics Reflected in Phase Space Representation

Surgical plane levels of isoflurane and ketamine induce calcium dynamics markedly different from those observed during quiet wakefulness (QW). Despite the high dose of anesthetic, we also observed several recordings that displayed dynamics similar to QW, which we referred to as 'awake-like'.

To characterize the differences in the dynamics and separate these recordings, we analyzed the corresponding Hilbert transforms. The Hilbert operator, $\hat{H}$, imparts a $\pi/2$ phase shift to each frequency of the real-valued signal $x(t)$, and returns the analytic signal $X(t) = x(t) + i\hat{H}[x(t)]$. We transform each pixel (*hilbert*, MATLAB), and plot the phase-space representations (i.e., when plotting $x(t)$ against $\hat{H}[x(t)]$) as a density plot. Such phase-space representations is particularly useful for oscillatory dynamics [2] as they appear as rings in phase-space.

Figures S3 through S5 show the Hilbert transform density plots, all normalized in the same way and with the same color axes for allow for direct comparison. Figure S3 shows two representative Hilbert transforms for

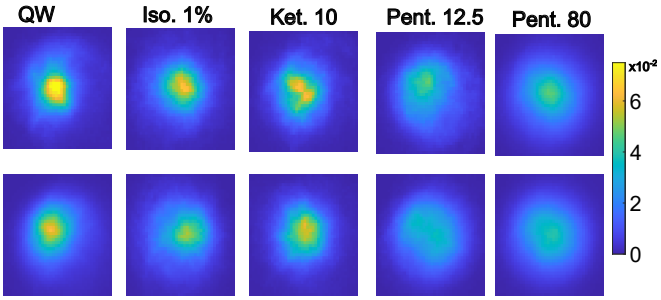

FIG. S3. Hilbert transform analysis of different drug cases. Representative Hilbert transform density plots for quiet wakefulness (QW), isoflurane 1%, ketamine 10 mg/kg, pentobarbital 12.5 and 80 mg/kg. Bottom and top rows are different recordings for the case specified at the top of column.

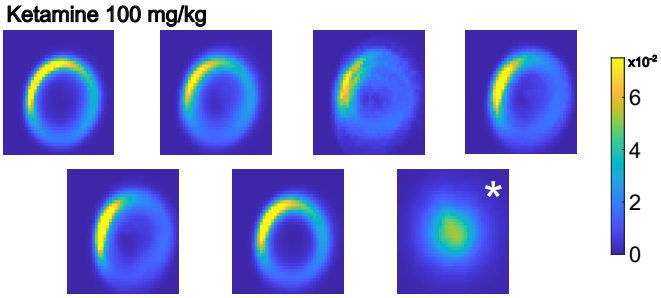

FIG. S4. Hilbert transform density plots for all seven ketamine 100 mg/kg recordings. Recording marked with an asterisk is awake-like.

QW. These were found to be roughly Gaussian shaped, reflecting the lack of characteristic oscillations. Likewise, all recordings of low-dose anesthetics, and pentobarbital 80 mg/kg, also had similar Hilbert transform profiles (Fig. S3). Surgical-plane levels of ketamine (100 mg/kg) induced prominent oscillations in the calcium dynamics of six out of seven recordings. These oscillations manifest as clear rings in phase space (Fig. S4). The final recording had no clear oscillations, and the corresponding Hilbert transform was similar to QW and thus labeled as awake-like (marked by asterisk in Fig. S4). On the other hand, seven of ten Isoflurane 2% recordings displayed small amplitude system-wide fluctuations, punctuated by brief system-sized (large amplitude) bursts. The remaining three recordings did not show these dynamics. The fluctuations manifest as sharp peaks in phase space where as the bursts appear as rings, with the prominence of the ring being related to the rate of bursting in the recording S5. Again, the three recordings for which this was not the case had phase space representations similar to QW (marked by asterisk in Fig. S5).

A. Avalanche Analysis of Surgical Plane Anesthesia Exhibiting Awake-Like Behavior

For the aforementioned awake-like recordings under surgical plane anesthesia (1 out of 7 for ketamine and 3 out of 10 for isoflurane), Fig. S6 shows both the calcium

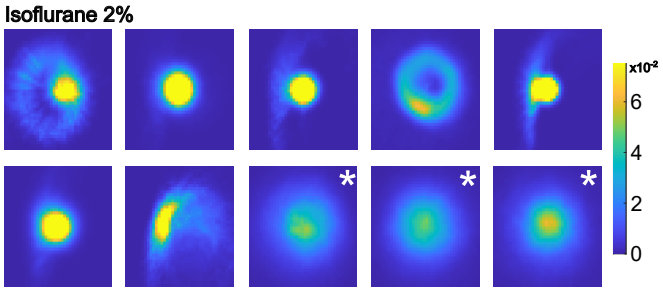

FIG. S5. Hilbert transform density plots for all ten isoflurane 2% recordings. Recordings marked with an asterisk are awake-like.

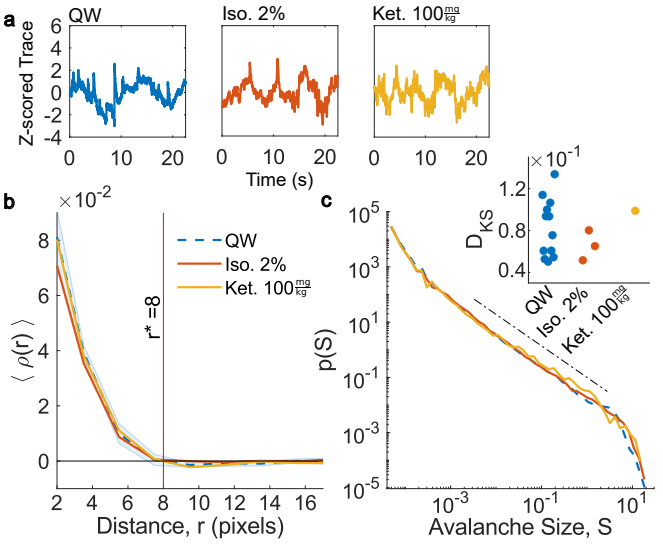

FIG. S6. Avalanche analysis of awake-like dynamics for surgical plane anesthesia. **a** Examples of (z-scored) traces of the total calcium activity. **b** The mean estimated PCF for awake-like isoflurane 2% (n =3) and ketamine 100 mg/kg (n = 1) with quiet wakefulness (QW) for reference. Shaded area denotes standard deviation of QW and is omitted from others for clarity. The vertical line shows the first zero crossing for QW. **c** Avalanche statistics along with QW for reference. Inset shows the KS distance between individual recordings, against the concatenated QW distribution. Source data are provided as a Source data file.

activity as well as the avalanche analysis. The corresponding avalanche initiations maps are shown in Fig. S7.

S4. Continuous Measurement of Heart Rate as Physiological Indicator of Anesthetic Depth

To monitor the anesthetic depth in animals over the course of our recordings, we extracted the heart beat from the original raw calcium signal in all cases. To do this, a global signal was generated by averaging across pixels. The global signal is filtered between 4 and 15 Hz (240 to 600 bpm), which was the same for all recordings for consistency. Peak detection was then used to determine the time between subsequent heart beats in order to extract the heart rate over time. To establish

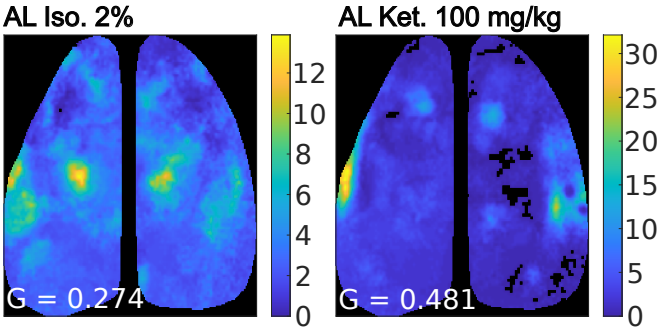

FIG. S7. Avalanche initiation maps as in Fig. 4 but for the awake-like conditions. Colorbars indicate the number of times a pixel was classified as an initiation site, averaged over all in-group maps, weighted by the number of observed avalanches with the Gini coefficient G indicated.

the robustness of our findings, we also used a continuous wavelet transform (*cwt*, MATLAB) as an alternative approach to estimate the heart rate and obtained very similar results. Examples of the extracted heart rate traces are shown in Fig. 5a. Fig. 5b shows the average heart rate and its variability for each recording. Our measurements show minimal variability and, hence, stationarity in this physiological indicator of anesthetic depth in animals with high-dose anesthesia over the course of a given recording. The average heart rates were found to be consistent with reports in the literature, though these too can vary and some cases (in particular ketamine 10 mg/kg and pentobarbital 12.5 mg/kg) have not been as broadly studied [3–10]. For each drug we compared the distribution of average heart rate values between QW, low dose, and high dose, and in each comparison the three were found to be statistically different from each other (one sided ANOVA test, isoflurane: $[F(2,22) = 110, p = 10^{-12}]$, ketamine: $[F(2,24) = 146, p = 10^{-14}]$, pentobarbital: $[F(2,19) = 44, p = 10^{-8}]$). We also tested whether awake-like recordings observed under high-dose anesthetics would exhibit heart rates different from their respective in-group recordings of high-dose anesthetics. This was not the case however, awake-like recording heart rates were consistent with other in-group recordings (hollow dots in Fig. 5b). This together with the stationary behavior of the heart rate for all animals with high-dose anesthesia is consistent with the observed time invariance of the avalanche statistics (see S6).

S5. Excitation-inhibition Balance Maps

While anesthetics can disrupt excitation-inhibition (EI) balance [11], it is not clear that this disruption would occur globally and uniformly across the cortex. To test this, we utilize a novel method to estimate EI balance from time series [12]. Briefly, this method uses an extension of the Critical Oscillations model of neuronal activity. By looking at changes in the envelope (obtained a Hilbert transform) they estimate a function EI balance measure, where $EI = 0$ means balance, $EI < 0$

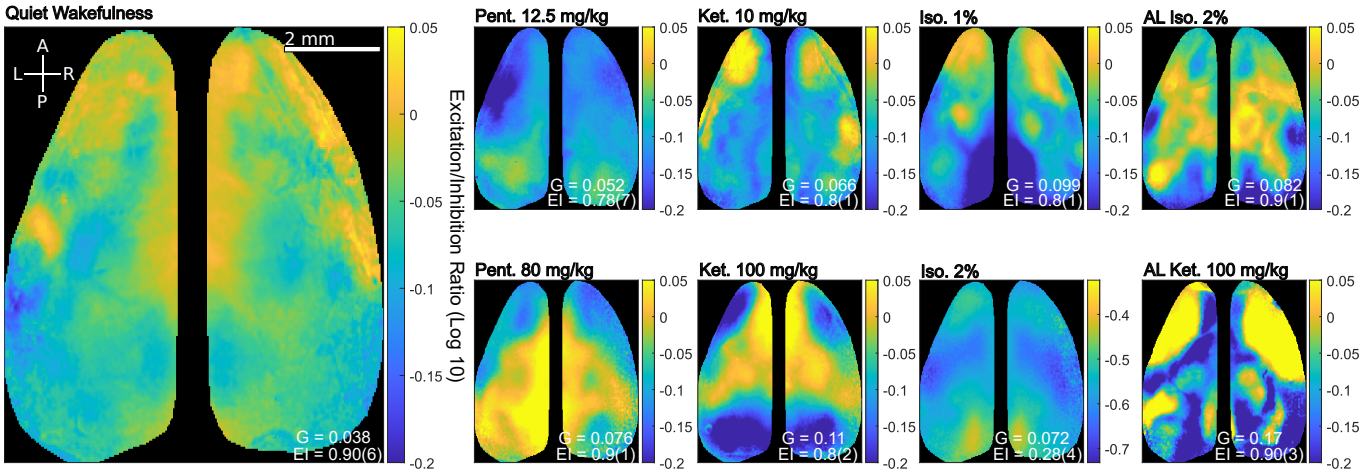

FIG. S8. Excitation-inhibition (EI) balance maps averaged over all animals belonging to a particular category. EI is the average (with standard deviation) over the field of view and G is the Gini coefficient. Color-bars show the (logarithmic) value of each color, with a value of EI < 1 means inhibition dominated while EI > 1 means excitation dominated.

means inhibition dominated, and $EI > 0$ means excitation dominated. Using the default settings provided in the public code, this analysis was conducted on a per-pixel basis, and averaged across in-group conditions to form the EI balance maps in Fig. S8. We emphasize that this method was developed for oscillatory signals EEG signals. While we believe the oscillatory nature of relative calcium fluctuations bares some similarity, our analysis based on wide-field optical imaging of calcium should be regarded as preliminary.

Caveats aside, as Fig. S8 shows for QW, the mean EI, averaged across pixels, is 0.90(6), which is close to the value of one expected in criticality [11, 12]. Importantly, this is distributed rather homogeneously across the cortical surface, as reflected in the small Gini coefficient (G, as shown in Eq. 3 of the main text). Anesthetics, however, can alter the EI map substantially in a multitude of ways. For example, both low-dose isoflurane and ketamine largely preserve EI globally, but locally EI is increased in the anterior, and for isoflurane decreased in the posterior. This decrease, which is not observed in ketamine, perhaps explains why isoflurane had such avalanche statistics essentially identical to QW. In high doses, ketamine preserves global EI balance but the distribution of EI is extremely heterogeneous, while isoflurane has an extremely low global EI. We also observe the awake-like recordings have a global EI nearly identical to QW, and their EI maps are drastically different from the predominant maps. Lastly, for completeness, pentobarbital is harder to classify. Low-dose maps suggest a greater reduction in global EI, while the high-dose sees an increase back to QW levels, but more localized than before.

S6. Temporal Invariance of Avalanche Statistics Over Course of Recording

We recorded additional three surgical-plane level ketamine and isoflurane recordings at twice the length of those used in the manuscript. Each recording was then divided in half into an early and late epoch and avalanche analysis was repeated for each epoch. These are shown in Fig. S9, and include for reference the avalanches in Fig. 3 (yellow curve), as well as a QW reference (dotted curve). We find that avalanche statistics between the early and late epochs are consistent with those reported in Fig. 3. This together with the observations in S3 indicates that the anesthetic depth is maintained over the course of each recording for the surgical-plane level anesthetics. Note that these longer recordings were not used for the results in the main manuscript.

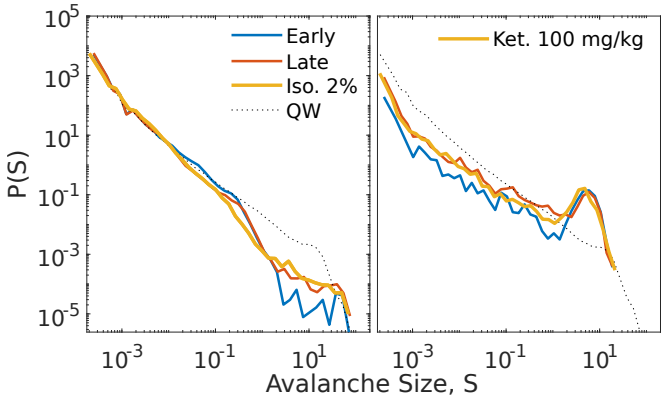

FIG. S9. Avalanche statistics for the early and late epochs for surgical plane isoflurane (left) and ketamine (right). Both the yellow and dot-dashed curve in each panel are the same as in manuscript and serve as reference. Source data are provided as a Source data file.

S7. Alternate Avalanche Definitions

Avalanches in the main text are defined by the clustering of pixels with above threshold signals, where the signal may be above threshold for multiple frames. An

alternative approach is to use a point-processed signal, where only the initial crossing of the threshold from below is used [13, 14]. Using the same interaction radius as in the main text ($r = 8$ pixels) and a per-pixel threshold of one standard deviation above the mean, we find distributions generated from point-processed signals follow the same distribution as those in the main text, albeit with a different cutoff (Figure S10). Additionally, one could use neighbouring pixels for clustering instead of a wider radius, such as in [14]. Fig. S11 shows this approach with both the non-point-processed and point-processed method, and we observe similar critical exponents.

Calcium signals have long decay times which could affect avalanche statistics. This is (partially) addressed by the point-processed approach, though a potentially more rigorous approach is to use deconvolution methods, which we did as well. We applied the code provided in [15], using default parameters. While deconvolution methods are primarily used in 2P imaging, the representative pixel in Fig. S12a shows the deconvolved signal appears rather faithful. Due to the computational time required for this method, we restricted our analysis to a single hemisphere of QW recordings. As each pixel collects bulk fluorescence from a $\sim 40 \mu m^2$ column of cortex, the pixel-wise signal represents the average calcium fluorescence of hundreds of neurons. Consequently the deconvolved signal estimates the multi-unit activity (MUA) of this population of neurons, and we extracted calcium transients or population 'spikes' from this MUA, which are shown in Fig. S12(a,c). We then repeated the avalanche analysis in the same manner as in the main manuscript. As Fig. S12d shows, the size distribution of calcium transients-derived avalanches is largely indistinguishable from the original distribution. Most importantly, the decay exponent (which is the relevant aspect for criticality) is statistically indistinguishable between the two cases. Avalanche durations also follow similar statistics as the original (Fig. S12e), albeit with a shift in the mean due to the calcium decay. In summary, regardless of which approach is used to define avalanches, our overall conclusions remain the same — power-law statistics in quiet-wakefulness are disrupted in a non-universal fashion by the different anesthetics.

S8. Alternate Hypothesis Testing

Common alternate hypothesis testing functions to power-law are exponential, stretched-exponential,and log-normal [1], all of which were tested. Of these, log-normal distributions were the closest to the power-law hypothesis and are shown in the main text. The other two distributions fared generally much worse and are shown in table SII. Note that for pentobarbital 12.5 and 80 mg/kg the analysis returned infinite values for the stretched-exponential estimation. This is likely due to the shallower slope of the two distributions, which is below 1 (assuming it is power-law). This results in the estimator used by *mle* (MATLAB) to return infinite values for the β parameter estimation, which could not be resolved.

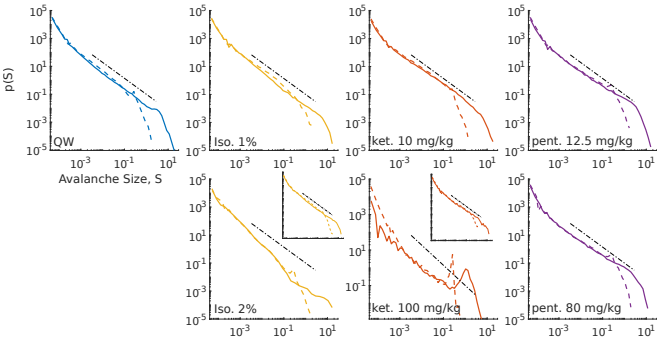

FIG. S10. Point-processed avalanche analysis. Comparison of distributions presented in main text (solid) with the point-processed versions (dashed). The dot-dashed line (same in every panel) corresponds to the estimated exponent for quiet-wakefulness (QW), along with the fitting domain. Insets show awake-like distributions for the corresponding condition. Source data are provided as a Source data file.

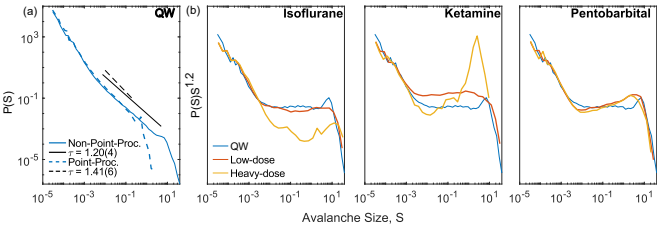

FIG. S11. Nearest-neighbour avalanche analysis. a) Quiet-wakefulness (QW) avalanches using adjacent pixels rather than the expanded neighbourhood used in the main paper. Distributions are shown for point-processed (dashed) and non-point-processed signals (solid), with their associated estimated exponents. b) The non-point-processed distribution from panel a) is compared against the equivalent distribution across different drug cases (not including awake-like cases). Each curve is rescaled to the $\tau = 1.2$ obtained in QW to show differences more clearly. Source data are provided as a Source data file.

S9. Connected Correlation Function

It has been suggested that at criticality the zero crossing of the connected correlation function, r_0, should scale linearly with the linear dimension of the box (at least up to $L/2$, where L is the system size) [16]. We do indeed observe linear scaling up to a window length close to 100 pixels (Fig. S13(a)), which is consistent with our system size. Note that our system size is limited – a box of around 200 × 100 pixels – as we need to exclude the right hemisphere due to the high symmetry. In addition, this box contains masked-out pixels that do not correspond to the cortical surface, roughly about 10%.

Interestingly, we find similar results for all conditions, i.e., there are neither significant differences between QW and the different drug conditions nor deviations from linear scaling (Fig. S13(b)). While naively one could take this as evidence that all high-dose cases can be considered

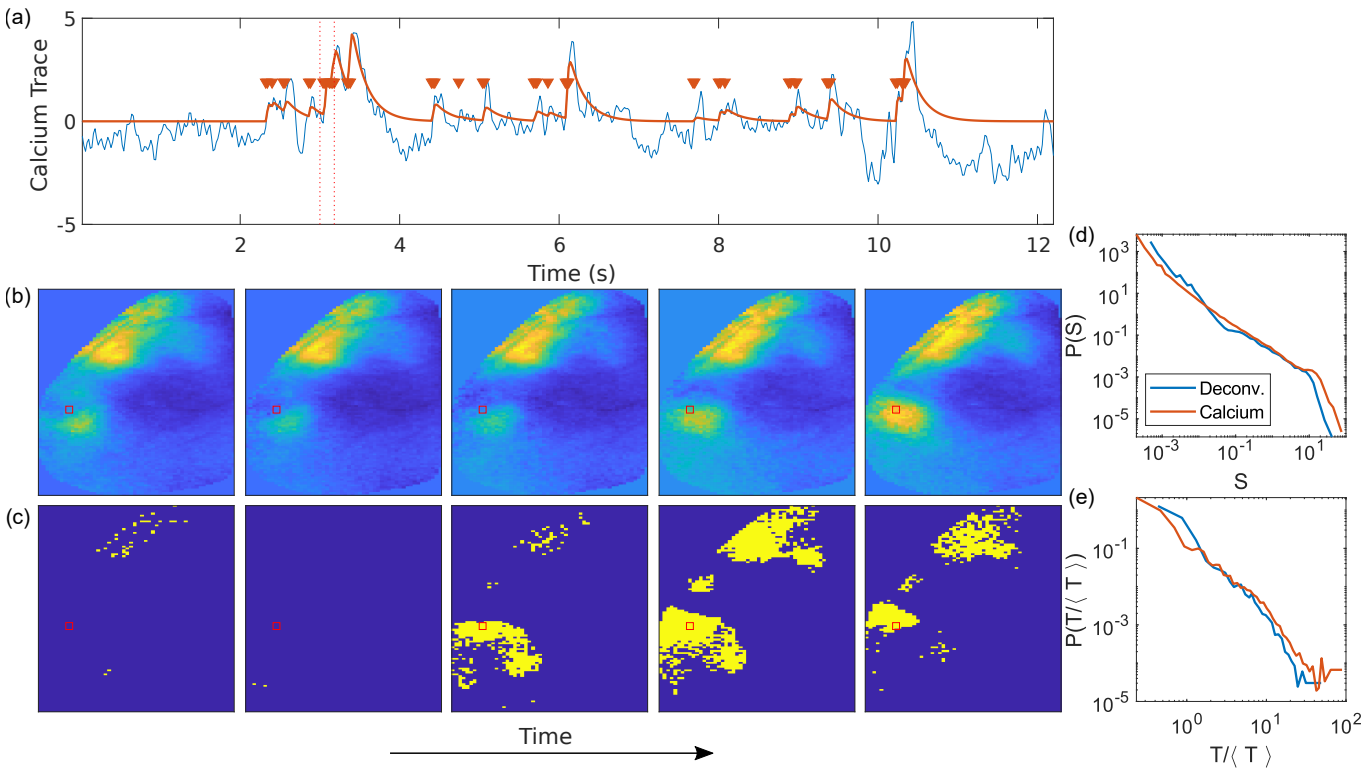

FIG. S12. Avalanche analysis on a deconvolved calcium signal. a) An example showing the original calcium signal (blue) along with the deconvolved signal (orange) for a single pixel. Triangles show times at which calcium transients were identified. Dotted-vertical lines show the segment where panels in (b) and (c) are taken from. b) Sample calcium transience signal over the FOV used in the original analysis (only a single hemisphere), with time going from left to right. Red square indicates the pixel corresponding to the trace in a). c) The calcium transients obtained from the deconvolved calcium signal for the same panels as in b). d) Avalanche sizes distributions obtained from the calcium transients shown in c) compared with the original calcium signal (concatenated over all quiet wakefulness recordings). e) Same as d) but for avalanche durations, re-scaled by their respective averages. Source data are provided as a Source data file.

	Exp (1)			StrExp (2)		
QW	856	1919	3775	20	81	210
Iso. 1%	491	654	2150	2	92	183
Iso. 2%	364	2658	4303	41	206	Inf
ket. 10 mg/kg	490	757	1552	1	16	98
ket. 100 mg/kg	-	2628	-	-	54	-
pent. 12.5 mg/kg	185	283	542	-2	18	Inf
pent. 80 mg/kg	158	271	540	2061	Inf	Inf

TABLE SII. Likelihood ratio test results for the exponential (Exp) and stretched-exponentioal (StrExp) alternative hypothesis. Only cases where plausibility of power-law for avalanche sizes can be established (*i.e.*, an exponent with $p > 0.1$ for a one-sample Kolmogorov-Smirnov distance test statistic) are considered. The numbers in the brackets indicate the number of estimated parameters for that distribution. The middle number in each cell denotes the median of the boot-strapping procedure, while the left and right numbers are the 10-*th* and 90-*th* percentiles. Note only one recording for Ketamine 100 mg/kg had an exponent with $p > 0.1$ and so uncertainties could not be established with this method.

critical — in contrast to our findings based on avalanche statistics — it is important to realize that within the small range of box sizes we have available, all of the sub/super/critical cases basically look the same — consistent with the work presented in [16]. Thus, the analysis of the correlation length scaling is not sensitive enough given our experimental limitations.

S10. Clustering Algorithm for Avalanches

Let Γ be the graph with N nodes, and $v_i(t) \geq 0$ be the signal at node $i \in [1, N]$ at discrete time $t \in [1, T_{max}]$. The set of graph-neighbours of i will be denoted $\Gamma(i)$. We assume there exists some set of times $\bar{T} \subset [1, T_{max}]$, for which $v_i(t \in \bar{T}) = 0$. We will use A_n to denote the n-th cluster.

1. At time t, find the set of active nodes: $S(t) = \{i\}$ such that $v_i(t) > 0$.

2. For all $i \in S(t)$, find the neighbours of i active in the previous time step: $\Omega_i(t-1) = \Gamma(i) \cap S(t-1)$. Depending on the size of $\Omega_i(t-1)$, three options are available. Either start a new avalanche, continue an existing avalanche, or merge multiple existing avalanches:

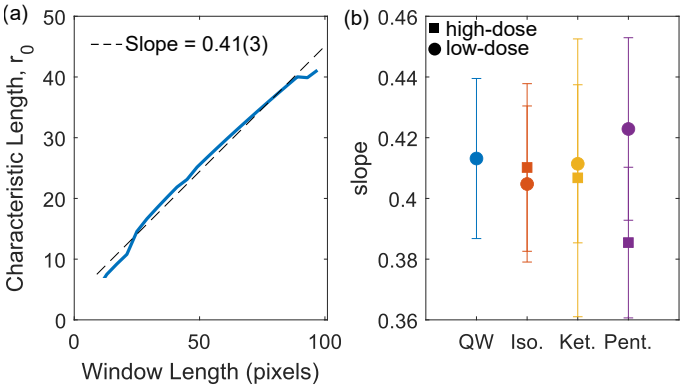

FIG. S13. Box-scaling analysis. (a) Characteristic length determined by the first zero crossing of the connected correlation function, as a function of the box window length, averaged across all quiet-wakefulness recordings. (b) Measured slope for all conditions, not including the high-dose cases do not including awake-like recordings. Source data are provided as a Source data file.

(a) if $\Omega_i(t-1) = \emptyset$, then i has no previously active neighbours which could explain its activation. Assume i is the start (root) of a new avalanche, labeled by A_n (n is arbitrary, but it can't have been previously used). The new avalanche has $v_i(t)$ and a start time of t.

(b) if $|\Omega_i(t-1)| = 1$, then i belongs to a previously existing avalanche, with an existing label A_n. Add i to A_n and add $v_i(t)$ to the size of A_n.

(c) if $|\Omega_i(t-1)| = m > 1$, then there exists m previously active neighbours. These m neighbours belong to a set of $n \leq m$ necessarily disjoint avalanches $\{A_{k_1}, ..., A_{k_n}\}$, where we assume the set is ordered so that $k_1 < k_2 < ... < k_n$. Merge the avalanches in the following way:

$$A_{k_1} \to A_{k_1} = \bigcup_{j=1}^{n} A_{k_j}.$$

The roots of the new A_{k_1} is the union of all the roots of the disjoint avalanches involved. The size of A_{k_1} is now the sum of all the sizes of the avalanches involved in the union, and the start of the avalanche, which is used to calculate its duration, is the minimum of the start times of the individual avalanches. All labels other than A_{k_1} can now be discarded and re-used. Finally, add i to the new A_{k_1}, and add $v_i(t)$ to the size of A_{k_1}.

3. Continue to time $t+1$.

At the end of the algorithm we have a set of M avalanches $\{A_{k_j}\}_{j=1}^{M}$. Each avalanche will have a set of participating nodes, the times at which they participated, a size (the sum of $v_i(t)$ across all nodes i at their times t), a duration (the number of time units the avalanche was active for), and a set of roots.

[1] Clauset, A., Shalizi, C. R. & Newman, M. E. Power-law distributions in empirical data. *SIAM review* **51**, 661–703 (2009).

[2] Davis, Z. W., Muller, L., Martinez-Trujillo, J., Sejnowski, T. & Reynolds, J. H. Spontaneous travelling cortical waves gate perception in behaving primates. *Nature* **587**, 432–436 (2020).

[3] Janssen, B. J. *et al.* Effects of anesthetics on systemic hemodynamics in mice. *American Journal of Physiology-Heart and Circulatory Physiology* **287**, H1618–H1624 (2004).

[4] Chu, D. K., Jordan, M. C., Kim, J. K., Couto, M. A. & Roos, K. P. Comparing isoflurane with tribromoethanol anesthesia for echocardiographic phenotyping of transgenic mice. *Journal of the American Association for Laboratory Animal Science* **45**, 8–13 (2006).

[5] Ewald, A. J., Werb, Z. & Egeblad, M. Monitoring of vital signs for long-term survival of mice under anesthesia. *Cold Spring Harbor Protocols* **2011**, pdb–prot5563 (2011).

[6] Constantinides, C., Mean, R. & Janssen, B. J. Effects of isoflurane anesthesia on the cardiovascular function of the c57bl/6 mouse. *ILAR journal/National Research Council, Institute of Laboratory Animal Resources* **52**, e21 (2011).

[7] Tsukamoto, A., Serizawa, K., Sato, R., Yamazaki, J. & Inomata, T. Vital signs monitoring during injectable and inhalant anesthesia in mice. *Experimental animals* **64**, 57–64 (2015).

[8] Low, L. A., Bauer, L. C. & Klaunberg, B. A. Comparing the effects of isoflurane and alpha chloralose upon mouse physiology. *PloS one* **11**, e0154936 (2016).

[9] Lee, C. & Jones, T. A. Effects of ketamine compared with urethane anesthesia on vestibular sensory evoked potentials and systemic physiology in mice. *Journal of the American Association for Laboratory Animal Science* **57**, 268–277 (2018).

[10] Kazdağli, H., Özel, H. F., Özbek, M., Alpay, Ş. & Alenbey, M. Classical heart rate variability and non-linear heart rate analysis in mice under na-pentobarbital and ketamine/xylazine anesthesia. *Turkish Journal of Medical Sciences* **52**, 858–869 (2022).

[11] Bellay, T., Klaus, A., Seshadri, S. & Plenz, D. Irregular spiking of pyramidal neurons organizes as scale-invariant neuronal avalanches in the awake state. *Elife* **4**, e07224 (2015).

[12] Bruining, H. *et al.* Measurement of excitation-inhibition ratio in autism spectrum disorder using critical brain dynamics. *Scientific reports* **10**, 9195 (2020).

[13] Scott, G. *et al.* Voltage imaging of waking mouse cortex

reveals emergence of critical neuronal dynamics. *Journal of Neuroscience* **34**, 16611–16620 (2014).

[14] Tagliazucchi, E., Balenzuela, P., Fraiman, D. & Chialvo, D. R. Criticality in large-scale brain fmri dynamics unveiled by a novel point process analysis. *Frontiers in physiology* **3**, 15 (2012).

[15] Pnevmatikakis, E. A. *et al.* Simultaneous denoising, deconvolution, and demixing of calcium imaging data. *Neuron* **89**, 285–299 (2016). URL `https://www.sciencedirect.com/science/article/pii/S0896627315010843`.

[16] Martin, D. A. *et al.* Box scaling as a proxy of finite size correlations. *Scientific Reports* **11**, 15937 (2021).